

# Spherical Balls Settling Through a Quiescent Cement Paste Measured by X-ray Tomography: Influence of the Paste Thixotropy

Subhransu Dhar <sup>1</sup>, Eduardo Machado-Charry <sup>2</sup>, Robert Schennach <sup>2</sup>, Teresa Liberto <sup>1</sup>, Agathe Robisson <sup>1\*</sup>

<sup>1</sup>Institute of Material Technology, Building Physics, and Building Ecology, TU Wien, Karlsplatz 13/207, 1040, Austria.

<sup>2</sup>Institute of Solid State Physics, TU Graz, Petersgasse 16/II, Graz, 8010, Austria.

\*Corresponding author(s). E-mail(s): [agathe.robisson@tuwien.ac.at](mailto:agathe.robisson@tuwien.ac.at);  
Contributing authors: [subhransu.dhar@tuwien.ac.at](mailto:subhransu.dhar@tuwien.ac.at);  
[machadocharry@tugraz.at](mailto:machadocharry@tugraz.at); [robert.schennach@tugraz.at](mailto:robert.schennach@tugraz.at);  
[teresa.liberto@tuwien.ac.at](mailto:teresa.liberto@tuwien.ac.at);

## Abstract

The settling of spherical balls in quiescent cement pastes of increasing age is studied. Metallic spheres with radii of 2, 2.5 and 3 mm are dropped into the paste and allowed to settle, while their position is tracked using X-ray tomography. The instantaneous velocity of the spheres, calculated from their movement, is observed to be quasi-constant during their fall, and an average is estimated. The results show that the average velocity of the balls decreases logarithmically with paste age until ball stoppage, for all three ball sizes. In parallel, the rheological properties of the cement paste are measured using a rheometer with a vane geometry. The evolution of the paste static yield stress over time is evaluated, and proves to be a reliable predictor for ball stoppage. Finally, thixotropic models of increasing complexity are evaluated. These models consider four forms of structural growth and breakdown parameters, and their ability to capture the ball settling velocity as a function of paste age is compared. This emphasizes the importance of considering paste breakdown in relation to shearing of the paste when the ball passes through it.

# 1 Introduction

Concrete remains an essential material for modern construction, due to its versatility, rapidly developing mechanical properties, and low cost coming from an optimized manufacturing process [1]. The binder holds together large particles such as sand and pebbles, and is typically a blend of ordinary Portland cement (OPC) and other more or less reactive particles [2]. The hydration reaction that transforms the fresh concrete (a fluid) into a strong solid comes from a dissolution and hydration/precipitation mechanism [3–5]. The binder, in its fresh state (before hardening), exhibits a complex rheological behavior, including thixotropy and shear-thinning or shear-thickening properties [6]. These rheological properties have to be controlled, especially in technological placements such as additive manufacturing [7–10]. The property of “thixotropy” refers to fluids that possess an internal structure that stiffens under quiescent conditions (fluid “at rest”), with growing elastic modulus and yield stress with time at rest, and that may return to a fluidized condition upon vibrating or high shear, i.e., under a load that disrupts their internal structure. In an ideal thixotropic fluid, these changes are fully reversible [11]. Pure cement pastes, as well as mixtures of OPC, have been described as thixotropic fluids, owing to the strong interparticle forces that develop between the hydrating cement particles [7, 12], and leads to the paste structuration. At rest, the particle network gets stronger and stiffer (due to flocculation and hydration), and under shear, it breaks down, giving the cement paste its thixotropic behavior. Properly characterizing concrete thixotropy is critical for optimizing its placement, predicting formwork removal time [13], and overall ensuring quality control in industrial processes. Among several methods to probe rheological properties (from field measurements such as funnel flow and cone spread [14, 15] to well-controlled lab rheometric tests [16, 17]), the study of sedimenting spheres in cementitious pastes may offer insights into its evolving microstructure and yield stress, and is inspired by work in other thixotropic fluids [18, 19]. The local flow induced by a sedimenting ball induces a local fluidization of the paste, that may or may not be enough to allow its further movement [20, 21].

The settling of particles within non-Newtonian fluids has been extensively studied, due to its relevance in industrial and natural processes [22]. In Newtonian fluids, Stokes’ law predicts terminal velocity based on fluid viscosity and solid-fluid density difference [23]. However, yield-stress fluids deviate significantly from this law: particles either settle continuously when the gravitational stress exceeds the yield threshold or arrest entirely once the fluid structural strength dominates [21]. The critical yield stress for particle arrest is derived from force balances, incorporating particle size, density contrast, and fluid rheology [18, 24, 25]. Experimental studies using spheres, cylinders, or disks have revealed complex velocity profiles, transient regimes, and wall effects [26–30]. Advanced imaging techniques, such as high-speed optical imaging [20], ultrasonic tracking [25], X-ray computed tomography [31] and magnetic resonance imaging (MRI) [32, 33], have enabled real-time tracking of particle (or bubble) trajectories, providing spatial and temporal resolution. The settling of spheres in aging yield stress fluids [19, 24, 30] and thixotropic fluids [20, 21, 34] has been the focus of several studies where paste aging (fluid structuration) and

paste fluidization are considered in models that can capture, at least partially, the sedimentation of particles in such complex fluids.

In this work, we explore yet another complex fluid, a cement paste, which rheological behavior displays thixotropy, with rapid structuration due to the flocculation of cement particles [35, 36]. To do so, the settling of spherical steel balls in a quiescent cement paste is investigated through X-ray computed tomography (X-Ray CT), and the ball velocity computed using image analysis. The test campaign focuses on the influence of cement paste age at rest. In parallel, the viscoelastic characterization of the paste is performed through small amplitude oscillatory shear, quantifying the evolution of the paste elastic modulus and static yield stress with paste age. Finally, thixotropic models of increasing sophistication are evaluated and their ability to properly capture the paste behavior discussed.

## 2 Materials and Methods

### 2.1 Sample preparation

Cement paste samples were prepared using Der Contragress cement (42.5 R,  $C_3A$ -free) in water, with a water-to-cement ratio (w/c) of 0.50, with 0.075% by weight of cement (bwoc) of polycarboxylether superplasticizer (Master Glenium ACE 430 from Master Builders), denoted SP, and 0.075% bwoc of retarder. The density of the cement paste was calculated from recipe using a density of 3150 kg/m<sup>3</sup> for the cement particles [37] and of 1000 kg/m<sup>3</sup> for the water, neglecting the additives, and amounts to 1835 kg/m<sup>3</sup>. For the settling ball experiments, batches of two liters of paste were mixed for each experiment. SP and retarder were pre-mixed in water and gradually added to the cement during mixing. Mixing was performed with an IKA® STARVISC 200-2.5 control overhead U-shaped stirrer at 800 rpm in two steps. First, the paste was mixed for 6 minutes, slowly adding water. Next, the paste was scraped from the sides of the container, and the mixture allowed to rest for 10 minutes. After 10 minutes, it was mixed again for 2 minutes at the same rpm. At the end of the 2 minute remix, the paste was immediately poured into the pipe designed for the settling experiments, and a timer started, with time elapsed described in the rest of the article as cement paste age. For rheology tests, cement paste samples were prepared in smaller amounts (80 ml) using the same IKA mixer. The 2-minute-remix was done within the cup of the vane geometry (at 800 rpm), after the same 10 minute rest time as above.

Small differences in the rheological behavior of the paste may arise from the different amounts of paste mixed but are considered minor in this work.

Time zero is defined, in the rest of the work, as the time right after the 2-minute-remix, and is sometimes called "paste age" throughout the manuscript, defining it as the elapsed time in paste under quiescent (or at rest) conditions.

### 2.2 Ball drop mechanism

Three different steel ball sizes of radii  $R$  2, 2.5 and 3 mm and density 7807 kg/m<sup>3</sup> were used. The ball drop mechanism consisted of an electromagnetic system which holds

the steel ball when the electricity is flowing through it. Upon breaking the electric circuit, the magnetic system is stopped and lets the ball fall. In order to correct for any positioning issue, a funnel system was added below the electromagnetic system, ensuring that the ball enters the paste very near the exact center of the pipe. The distance between the ball attached to the magnet and the surface of the cement slurry was about 70 mm. The ball therefore entered the paste with a non-negligible velocity, which was useful for overcoming the paste "skin" -a layer of drying cement paste that may form at higher paste age-, ensuring that the ball penetrates the bulk of the paste. The behavior of the ball right below the surface was not considered.

### 2.3 Imaging the falling ball with an X-Ray CT scanner

The setup was custom-made with a Plexiglas tube of 70 mm diameter and height of 550 mm, fixed on a wooden board to reach a verticality of  $\pm 0.5^\circ$ . Plexiglas was chosen to mitigate X-ray absorption and the pipe diameter to reach a tube-to-ball diameter ratio of at least 10. The CT scanner was UniTOM XL from TESCAN. Optimizing the CT scan resolution and the distance to sensor lead to a window of observation of 300 mm height, so that the ball falling could be observed from cement top interface to about 300 mm penetration depth. A schematic of the setup is shown in Fig. S1 of SI.

The steel ball was released at different ages of the paste, between 120 s (the minimum time to pour the cement paste in the tube and place it in the X-Ray chamber) and 480 s, time at which the biggest ball stopped settling during the experiment, at increment of 60 s. For each ball size and age of paste, a new freshly mixed paste was used (no successive ball falling in a single sample was explored here), and the experiment was repeated between 2 and 5 times, depending on the test reproducibility. The ratio of the tube-to-ball diameter was 11.7 for the biggest ball, allowing us to neglect wall effects [38, 39]. Bottom wall effects could also be neglected, as observations were made at least 150 mm above the cell bottom.

Results are shown for balls which velocity could be resolved at the frequency of acquisition (25 images per second), e.g., the ball of 3 mm diameter was sedimenting too fast in the paste with 120 s aging time. When ball stoppage was observed, it was typically preceded by a decrease in its velocity. If the ball was observed to stop within the observation window, its velocity is displayed as zero. Error bars were calculated as data standard deviation, considering all experiments.

### 2.4 Ball tracking and velocity calculation

The set of images recorded during the experiments was optimized for brightness and contrast using ImageJ [40]. The ball was then automatically localized using video spot tracker software from CISMM. The surface of the cement paste is taken as zero value of the vertical axis. The position of the ball at each frame was recorded, the time between two image frame being  $\Delta t = 0.04$  s. A central differential formula using one time step below and above was used to calculate the instantaneous velocity of the sphere.

## 2.5 Rheological measurements

The rheological measurements were performed using an Anton Paar 302 rheometer with a vane (4 blade) in sanded cup geometry, described in [36]. The temperature was set to 25 °C to match the temperature inside the CT scanner.

The rheological protocol, shown in Fig. 1, consisted of three steps, and was applied right after the remix phase of the paste, described in 2.1.

During the first step, a small amplitude oscillatory shear of  $\gamma = 10^{-5}$  was applied for a duration of 600 s, and used to follow the storage modulus  $G'$  as a function of time. Within this period and at intervals of 60 s, amplitude sweeps up to a strain amplitude of  $\gamma = 10^{-4}$  were imposed to the paste. This step enables the estimation of an elastic modulus  $G'_{lin}$ , taken as the average of the storage moduli in the linear elastic region, and the determination of a critical strain  $\gamma_{cr}$ , value of the strain amplitude at which the value of  $G'$  decreases to 80% of  $G'_{lin}$ . This step is conducted while minimally altering the microstructure of the paste, an hypothesis confirmed when tests without the amplitude sweeps were performed, and showed a similar  $G'$  evolution with time (see Fig. 3). From  $G'_{lin}$  and  $\gamma_{cr}$ , a static yield stress  $\tau_s = \gamma_{cr} \cdot G_{lin}$  was determined as a function of paste age.

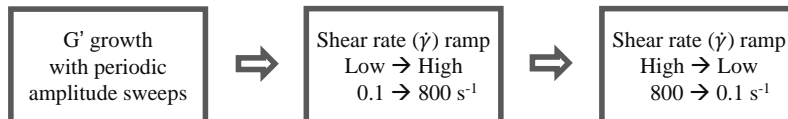


**Fig. 1:** Rheology protocol used to study the cement paste.

The second step consisted of a shear rate ramp from low to high, and is used to fluidize the sample. The fluidization of the paste is considered to erase its history in the time frame considered in this work (10 minutes), the structuration of the paste being quasi reversible in this region [35]. The shear rate equivalent values are proposed by Anton Paar and given equal to the rotational velocity in rpm.

The third step, the ramp from high to low shear rate, is used to measure the apparent dynamic viscosity of the paste as a function of shear rate, and the plateau value between 400 and 800  $s^{-1}$  is chosen to describe the fully fluidized paste shear viscosity. A Herschel-Bulkley model is also fitted on the data to identify the paste dynamic yield stress (in SI).

## 3 Rheological characterization results

### 3.1 Viscosity evaluation

From the shear ramps, the viscosity of the paste is shown to plateau between 400 and 800  $s^{-1}$  to reach a viscosity of  $1 \pm 0.1 \text{ Pa.s}$ , as shown in Fig. 2. At this very early age, the fluidized behavior of the paste is considered independent of its age, as long as fluidization is conducted through high shear, confirmed by the near superposition

of the ramps up and down. From the Herschel-Bulkley model fit, the paste dynamic yield stress was identified to be 33 Pa (see Fig. S3 of SI).

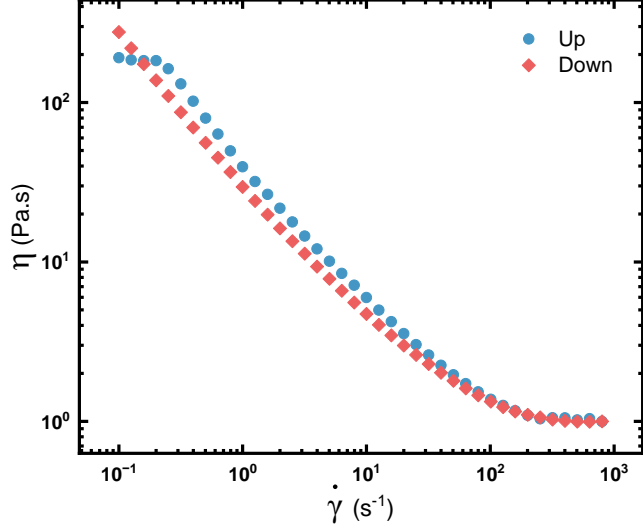


**Fig. 2:** Cement paste viscosity as a function of shear rate from flow test

### 3.2 Growth of storage modulus $G'$ and complex viscosity $\eta^*$ as a function of paste age

Fig. 3 shows the growth in storage modulus  $G'$  as a function of time (or paste age), obtained from the protocol with regularly imposed amplitude sweeps (2 independently mixed samples), and from the protocol without. This confirms that the amplitude sweep minimally disrupts the paste, and its structuration with time at rest.

From the measurements of storage and loss moduli, resp.  $G'$  and  $G''$ , the complex viscosity  $\eta^* = \frac{\sqrt{G'^2 + G''^2}}{\omega}$ , with  $\omega$  the angular frequency [41], was evaluated, and is plotted in Fig. 4 as a function of time.

The data can be fitted by a simple equation, that captures the paste structuration, with the form:

$$\eta^* = \eta_o^* + K \cdot t^m \quad (1)$$

where  $\eta_o^*$  is the complex viscosity of the paste at time  $t=0$ , and  $K$  and  $m$  are material parameters.

The fit of Eqn. 1 on experimental data returned the parameters shown in the inset of Fig. 4.

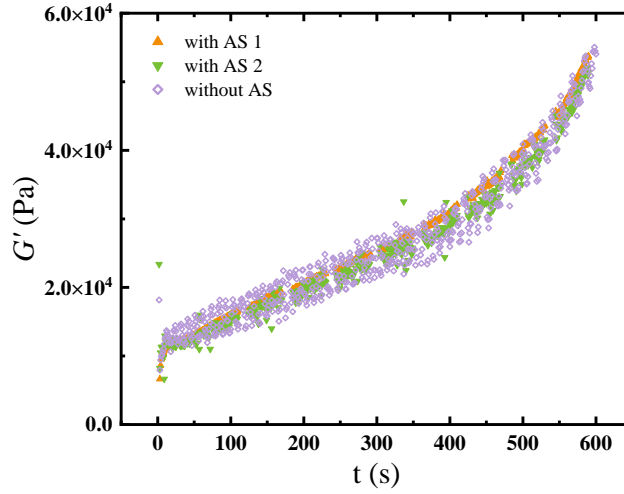


**Fig. 3:** Growth of storage modulus  $G'$  with time (or paste age). The trials with amplitude sweep (AS) are shown with orange upward triangles and green downward triangles. The trial without any amplitude sweep is shown by purple diamonds.

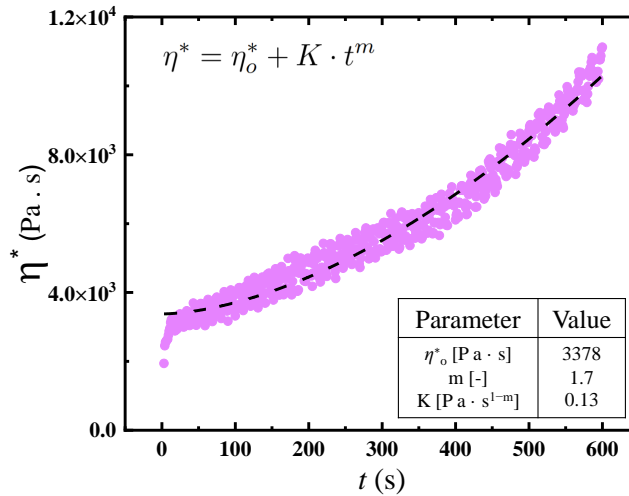


**Fig. 4:** Growth of complex viscosity  $\eta^*$  as a function of time  $t$  (or paste age) represented by purple dots. The dashed line shows the fit of the equation  $\eta^* = \eta_o^* + K \cdot t^m$ .

### 3.3 Amplitude sweep and evaluation of the growth of static yield stress $\tau_s$ with time

Amplitude sweeps, performed every 60 s at paste ages between 120 and 600 s, are shown Fig. 5(a). The evolution of the static yield stress of the paste  $\tau_s$  obtained from strain sweep characterization is shown in Fig. 5(b).

The growth in  $\tau_s$  with time is fitted with a linear equation and returns:

$$\tau_s(t)[Pa] = 0.026 [Pa.s^{-1}] \cdot t [s] + 3.55 [Pa] \quad (2)$$

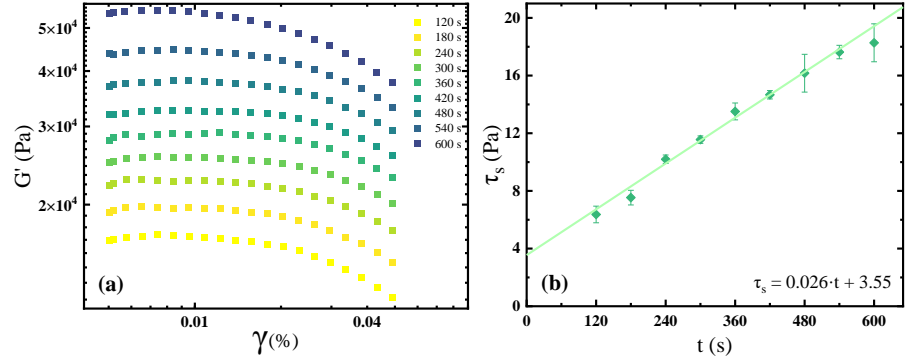


**Fig. 5:** (a) Amplitude sweep at different aging times showing the drop of storage modulus  $G'$  as a function of increasing strain amplitude  $\gamma$ . The gradient of color from light yellow to dark purple depicts increasing aging time from 120 to 600 s. (b) Growth of static yield stress  $\tau_s$  as a function of age  $t$  of the cement paste (green diamonds). The error bars represent the range (maximum-minimum) for two independent trials. The fitted green line shows a linear fit and returns  $\tau_s = 0.026 \cdot t + 3.55$ .

## 4 Ball settling results: Ball velocity and ball stoppage in the cement paste as a function of its age

The results of ball localization within the 300 mm observation window are shown in Fig. 6 for the 3 ball sizes  $R = 2, 2.5$  and  $3$  mm, at cement paste age between 120 and 480 s, i.e., in all conditions where the ball was moving through the window, and where enough data could be acquired. Test repeats are plotted, showing an acceptable reproducibility of the results.

The instantaneous velocity  $v_i$  of the ball as a function of its position was derived from the above data, and is shown in Fig. 7. After the initial first few seconds, the ball attains a steady-state velocity, where the velocity remains almost constant during the window of observation, showing that paste aging is negligible during the ball falling. The velocity was only observed to decrease during the ball settling in cases where the ball stopped within the window of observation (see Fig. S4 in SI).

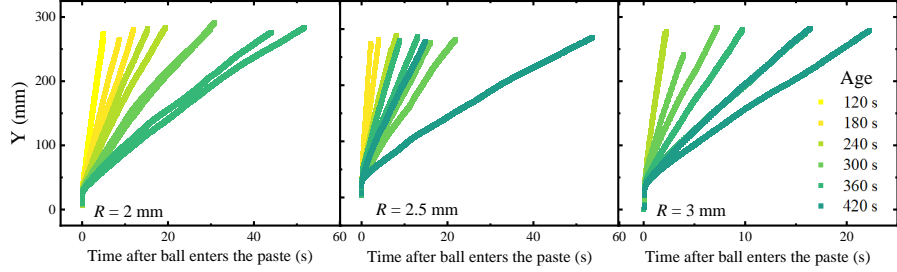


**Fig. 6:** Measured vertical position of falling ball as a function of time, for various cement paste ages and ball radii (2 mm -left graph-, 2.5 mm -middle graph- and 3 mm -right graph-), for 2 independent trials in each condition. Time is here defined as the time elapsed since the ball is first recorded to touch the cement paste. The gradient of color from light yellow to dark green represents increasing paste age of the cement paste, from 120 to 420 s. The aging time at which the ball stopped within the region of observation is not shown here.

The steady-state velocity  $v$ , calculated by averaging the instantaneous velocity values  $v_i$  at ball positions between 100 and 225 mm, was plotted as a function paste age (taken as the time at the beginning of the experiment) in Fig. 8. The data points corresponding to paste age at which the ball was observed to stop were added as data points with  $v = 0 \text{ m.s}^{-1}$ . The data shows that  $v$  decreases logarithmically with paste age, until the ball stops.

The particle Reynolds numbers were estimated using the measured ball settling velocities and the equation for the average shear rate around the sedimenting ball  $\dot{\gamma} = v/R$  (with  $v$ , ball settling velocity and  $R$  ball diameter) [32], and remain in all cases below 0.4.

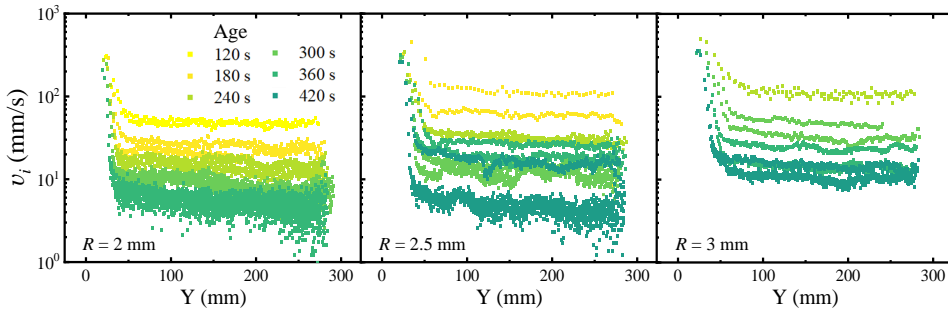


**Fig. 7:** Measured instantaneous velocities of falling balls  $v_i$  as a function of vertical position  $Y$  of the ball for different aging times of the cement paste and ball radii. The gradient of color from light yellow to dark green represents increasing aging time of the cement paste, probed between 120 and 420 s. Two test repeats are shown.

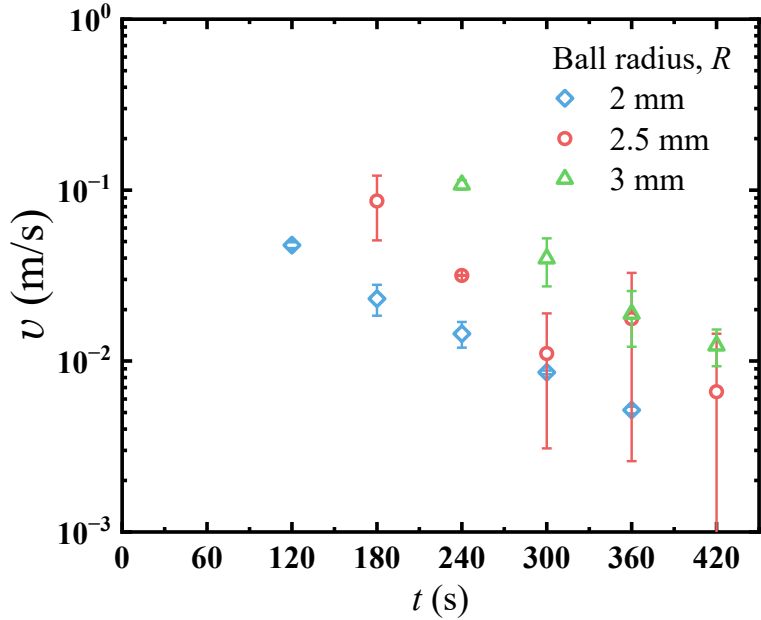


**Fig. 8:** Experimental steady state velocity  $v$  of the falling balls as a function of the paste age  $t$  at the start of the ball falling experiment, in a log-lin scale. Three ball sizes are used with radii 2 mm (blue diamonds), 2.5 mm (red dots) and 3 mm (green triangles). The error bars represent the data standard deviation.

## 5 Theory: Sedimenting ball in a thixotropic fluid

### 5.1 Theory: Velocity of a sphere falling through a quiescent aging thixotropic fluid

The terminal velocity  $v$  of a sphere falling through a Newtonian fluid is given by Stoke's equation [23]:

$$v = \frac{2}{9} \frac{(\rho_{sphere} - \rho_{paste})gR^2}{\eta} \quad (3)$$

With  $R$ , the radius of the ball,  $g$ , the acceleration due to gravity,  $\rho_{ball}$ , the density of the ball,  $\rho_{paste}$ , the density of the fluid and  $\eta$ , the viscosity of the fluid.

The equation is valid for Reynolds number  $Re \ll 1$ , but acceptable for  $Re < 1$  [42].

In thixotropic fluids, the viscosity  $\eta$  does not remain constant, and can be described as a function of a structure parameter  $\lambda$  [43]:

$$\eta(\lambda) = \eta_o(1 + \lambda^n) \quad (4)$$

where  $\eta_o$  is the viscosity of the fluid in its fully fluidized form (or fully de-structured, i.e., when  $\lambda = 0$ ), and the exponent  $n$ , a material parameter.

The structure parameter  $\lambda$  can be split into a structural growth parameter  $\lambda_g$  and a breakdown parameter  $\lambda_b$  [21], independent of each other, giving

$$\lambda = \lambda_g + \lambda_b \quad (5)$$

The new equation for viscosity can then be introduced back into the Stokes equation to obtain the terminal velocity of a sphere falling through the thixotropic material [21], giving:

$$v = W[1 + (\lambda_g + \lambda_b)^n]^{-1} \quad (6)$$

with

$$W = \frac{2}{9} \frac{(\rho_{ball} - \rho_{paste})gR^2}{\eta_0} \quad (7)$$

In this work, we aim at exploring the aspects of cement paste thixotropy that control the sphere settling velocity, and we therefore consider different expressions of the structural parameter  $\lambda$ . Using literature, we consider two different expressions of the structural growth parameter  $\lambda_g$ , and two different expressions of the breakdown parameter  $\lambda_b$ . Below, we write the equations to within a constant, i.e., the constants of integration are not displayed as they are in the works that inspire this study [21]. The expressions are described below:

#### Expression 1 for the structure growth parameter $\lambda_{g1}$

Here, the structure parameter  $\lambda_g$  is assumed to grow linearly with time (or paste age) [7], thus

$$\lambda_{g1}(t) = \frac{t}{T} \quad (8)$$

with  $T$  a characteristic time (unit [s]), property of the material.

#### Expression 2 for the structure growth parameter $\lambda_{g2}$

Here, the growth structure parameter  $\lambda_{g2}$  is assumed to change as the complex viscosity  $\eta^*$  measured under oscillatory shear [44–46]. The temporal evolution of  $\lambda_{g2}$  is then written in the form of the temporal evolution of  $\eta^*$  (Fig. 4 and Eqn. 1), as

$$\lambda_{g2} = \frac{K}{\eta_o^*} \left( \frac{t}{T'} \right)^m \quad (9)$$

with  $T'$  a characteristic unit less time (unit [-]), property of the material, and  $\eta_o^*$ ,  $K$  and  $m$ , the values identified from rheological tests and shown in Fig. 4.

Similarly, the breakdown structure parameter  $\lambda_b$  can be written using two different expressions:

**Expression 1 for the structure breakdown parameter  $\lambda_{b1}$**

Here, the ball movement through the paste is assumed to affect only a small volume of the paste around it, and its effect is neglected. In other words, the passage of the ball is presumed to have no effect on the paste breakdown:

$$\lambda_{b1} = 0 \quad (10)$$

**Expression 2 for the structure breakdown parameter  $\lambda_{b2}$**

Following the work of Biswas et al. [20], we use an expression of the structure breakdown parameter that evolves proportionally to the ball diameter and time, and follows

$$\lambda_{b2} = -\varepsilon(2 \cdot R)t \quad (11)$$

with  $\varepsilon$  a material parameter, with unit  $[m^{-1} \cdot s^{-1}]$ .

The negative sign indicates the drop in viscosity linked to the breakdown of the paste.

Based on the four expressions above, we can write four cases for the expression of the structure parameter  $\lambda$ , re-introducing the constant of integration as  $\lambda_o$ . From there, four expressions of the settling ball velocity  $v$  are proposed, denoted using Roman numbers:

**Case I  $\lambda_I = \lambda_{g1} + \lambda_{b1}$ :**

Here, the growth structure parameter increases with time  $t$  as  $1/T$  and the breakdown structure parameter is zero. Hence, the structure parameter becomes:

$$\lambda_I = \frac{t}{T} + \lambda_o \quad (12)$$

$\lambda_o$  represents the initial structure parameter of the material.

The velocity becomes:

$$v_I = W \left[ 1 + \left( \frac{t}{T} + \lambda_o \right)^n \right]^{-1} \quad (13)$$

**Case II  $\lambda_{II} = \lambda_{g1} + \lambda_{b2}$ :**

Here, the growth structure parameter increases with time  $t$  as  $1/T$  and the breakdown structure parameter increases linearly with time and ball radius  $R$ . Hence, the structure parameter becomes:

$$\lambda_{II} = \frac{t}{T} - \varepsilon(2 \cdot R)t + \lambda_o \quad (14)$$

The velocity becomes:

$$v_{II} = W \left[ 1 + \left( \frac{t}{T} - \varepsilon(2 \cdot R)t + \lambda_o \right)^n \right]^{-1} \quad (15)$$

**Case III**  $\lambda_{III} = \lambda_{g2} + \lambda_{b1}$

Here, the growth structure parameter increases with  $t^m$  and the breakdown structure parameter is zero. Hence, the structure parameter becomes:

$$\lambda_{III} = \frac{K}{\eta_o^*} \left( \frac{t}{T'} \right)^m + \lambda_o \quad (16)$$

The velocity becomes:

$$v_{III} = W \left[ 1 + \left( \frac{K}{\eta_o^*} \left( \frac{t}{T'} \right)^m + \lambda_o \right)^n \right]^{-1} \quad (17)$$

**Case IV**  $\lambda_{IV} = \lambda_{g2} + \lambda_{b1}$

Here, the growth structure parameter increases with  $t^m$  and the breakdown structure parameter increases linearly with time and ball radius  $R$ . Hence, the structure parameter becomes:

$$\lambda_{IV} = \frac{K}{\eta_o^*} \left( \frac{t}{T'} \right)^m - \varepsilon(2 \cdot R)t + \lambda_o \quad (18)$$

The velocity becomes:

$$v_{IV} = W \left[ 1 + \left( \frac{K}{\eta_o^*} \left( \frac{t}{T'} \right)^m - \varepsilon(2 \cdot R)t + \lambda_o \right)^n \right]^{-1} \quad (19)$$

In cases I to IV,

$$W = \frac{2}{9} \frac{(\rho_{ball} - \rho_{paste})gR^2}{\eta_0} \quad (20)$$

## 5.2 Theory: Ball stoppage in a yield stress fluid

Beris and co-authors derived an infinite drag coefficient from the analysis of the yielded and unyielded regions of a sphere settling through a Bingham fluid [18]. It was linked to settling ball stoppage in various yield stress fluids [24, 32], and lead to the inequality (21), which describes the conditions under which a settling ball ceases to move.

$$\frac{\tau_y}{(\rho_{ball} - \rho_{paste}) \cdot g \cdot 2R} \geq \frac{1}{21} \quad (21)$$

where  $\tau_y$  is the yield stress of the fluid,  $\rho_{ball}$  and  $\rho_{paste}$  are the densities of the ball and the paste respectively, and  $R$  is the radius of the ball.

## 6 Model fit on experimental data: Results and discussion

### 6.1 Model to predict the velocity of balls of various diameters falling through the quiescent aging cement paste

The experimental values of the settling sphere velocity in cement paste shown in Fig. 8 are used to fit the equations developed for case I (linear increase of structure growth parameter with time and no consideration of breakdown), case II (linear increase of structure growth parameter with time, and linear decrease of breakdown parameter with time), case III (non linear increase of structure growth parameter with time and no consideration of breakdown) and case IV (non linear increase of structure growth parameter with time and linear decrease of breakdown parameter with time).

For the identification, the following constants were used:  $g = 9.81 \text{ m/s}^2$ ,  $\rho_{ball} - \rho_{paste} = 5972 \text{ kg/m}^3$ , and  $\eta_0 = 1 \text{ Pa} \cdot \text{s}$  (viscosity of the paste at the highest shear rate tested, around  $\dot{\gamma} \approx 800 \text{ s}^{-1}$ , see Fig. 2).

In addition, the initial structure parameter of the material, represented by  $\lambda_o$ , was considered to be near zero as the material was sheared at a high rate just before the start of the experiment, and is considered fully fluidized. For this study, it was arbitrarily set to 0.01 (a small value after heavy mixing, but not zero to prevent convergence issues).

During the fitting procedure, all three remaining material parameters ( $n$ , the exponent,  $T$  or  $T'$ , a characteristic time, and  $\varepsilon$ , a proportionality factor) were identified. The results are shown Tab. 1, with R-square values.

**Table 1:** Identified parameter values identified on the integrality of the settling experiments

Parameter / Case	Case I	Case II	Case III	Case IV
$n$ [-]	4.80	3.49	2.82	1.11
$T$ [s] or $T'$ [-]	220.41	131.06	0.56	0.20
$\varepsilon$ [ $\text{m}^{-1} \cdot \text{s}^{-1}$ ]	-	0.59	-	4.22
R-square	0.56	0.70	0.56	0.91

Results of the identification are shown on a 2D graph Fig. 9. The 3D fits of cases I-IV (time, ball radius and velocity) are shown in Fig. S2 of SI. The R-square value of 0.91 obtained for case IV shows the importance of considering paste breakdown in

relation to shearing of the paste when the ball passes through it.

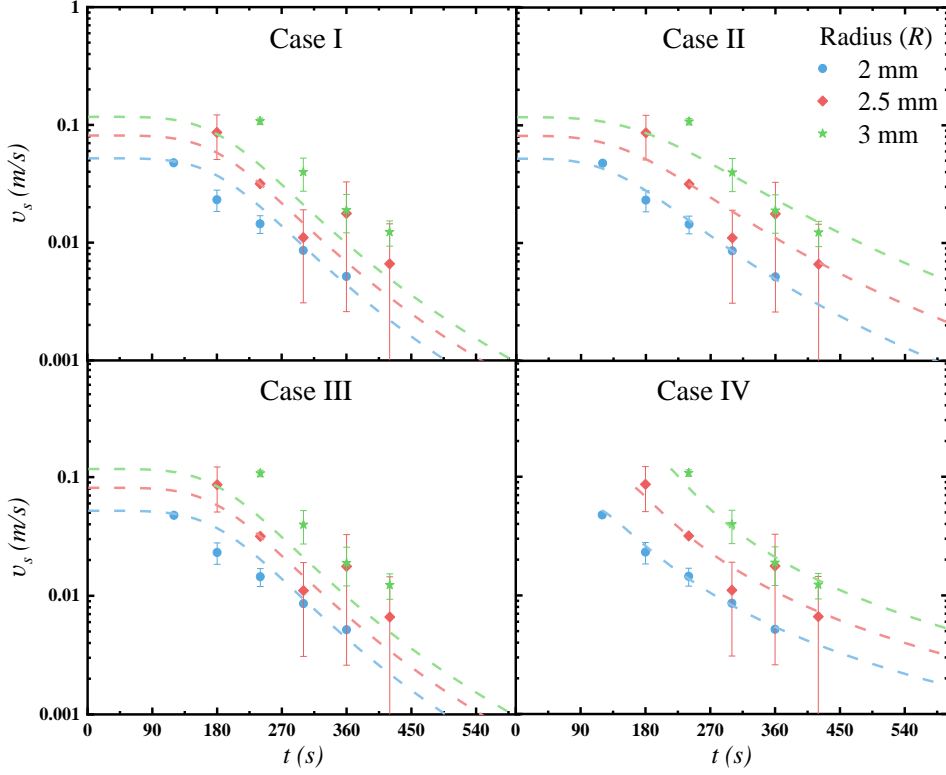


**Fig. 9:** Experimental (dots) and theoretical (lines) ball settling velocities for the models I to IV, in log-lin scale. Models were fitted with 2 parameters for cases I and III, and 3 parameters for cases II and IV. The error bars in data represents the data standard deviation.

The models of cases II and IV fit the experimental data better than the other models, showing the importance of considering the cement paste destructure (or fluidization) that occurs at the passage of the ball.

The characteristic times  $T$  of order 100 s identified using the linear structuration growth model (cases I and III) seem aligned with studies on cement (e.g., [47]), but a detailed discussion on characteristic time scales of thixotropic materials [48] is beyond the scope of this work.

## 6.2 Prediction of the ball stoppage in an aging cement paste

From Eqn. 21, and using  $\rho_{ball} - \rho_{paste} = 5972 \text{ kg/m}^3$ , and the three radii  $R$  of the balls (2, 2.5 and 3 mm), the yield stresses corresponding to ball stoppage could be calculated and are shown in Tab. 2.

The static yield stress of the paste in the time window where ball stoppage occurred could also be estimated from the rheological characterization (Fig. 5), and is shown in Tab. 2 too.

**Table 2:** Theoretically estimated yield stress of cement paste for ball stoppage (Eq. 21) & experimentally measured static yield stress at time of stoppage (Fig. 5 and 8)

Ball radius (mm)	Theo. $\tau_y$ (Pa)	Exp. $\tau_s$ (Pa)
2.0	11.2	12.9-14.5
2.5	14.0	12.9-14.5
3.0	16.7	14.5-16.0

It is important to note here the value of the dynamic yield stress measured from flow curve (33 Pa, see Fig. S3 in SI) does not seem to be quantitatively related to ball stoppage. As such, the cement paste static yield stress is a better predictor of ball stoppage than the dynamic yield stress. It is unsurprising, as the falling ball shears the paste from an "at rest" state to a fluidized state. Nevertheless, as  $\tau_s$  was measured from small amplitude oscillatory strain, it tends to show that the ball movement induces only limited and very localized paste yielding.

## 7 Conclusion

This study investigated the settling of spherical balls through cement pastes of increasing age (at rest). The balls were made of metal and three different radii (2 mm, 2.5 mm and 3 mm) were tested. The results show that the average velocity of the balls decreases logarithmically with the age of the cement, until the balls stop moving within the paste, a behavior that has been observed in other thixotropic materials. Inspired by works on thixotropic fluids and aging yield stress fluids, a model was developed that considers both structural growth and breakdown parameters. After identifying three material constants by fitting the experimental data, a reasonable fit was obtained, demonstrating the adequacy of the developed theories in modeling cement pastes, and the importance of taking the paste destructuration into account. Finally, ball stoppage could be predicted when the static yield stress, as measured by small-amplitude oscillatory shear, was considered.

## 8 Acknowledgements

The work was supported by Österreichische BautechnikVereinigung (ÖBV) and Österreichische Forschungsförderungsgesellschaft (FFG) (Project number 870962). The authors thank C. Barentin and R. Biswas for fruitful discussions, and J. Kirnbauer and M. Ramizi for their help during the experimental campaign. Authors also acknowledge TU Wien Bibliothek for financial support through its Open Access Funding Program.

## References

- [1] M.F. Ashby, *Materials and sustainable development* (Butterworth-Heinemann, 2022)
- [2] European Committee for Standardization (CEN). Cement – Part 1: Composition, specifications and conformity criteria for common cements (2023). Defines 27 common cement types and constituents
- [3] J.W. Bullard, H.M. Jennings, R.A. Livingston, A. Nonat, G.W. Scherer, J.S. Schweitzer, K.L. Scrivener, J.J. Thomas, Mechanisms of cement hydration. *Cement and concrete research* **41**(12), 1208–1223 (2011)
- [4] E. Gartner, J. Young, D. Damidot, I. Jawed, *Hydration of Portland Cement* (2001), pp. 57–113
- [5] K. Ioannidou, M. Kanduč, L. Li, D. Frenkel, J. Dobnikar, E. Del Gado, The crucial effect of early-stage gelation on the mechanical properties of cement hydrates. *Nature communications* **7**(1), 12106 (2016)
- [6] P.F.G. Banfill, *Rheology of Fresh Cement and Concrete: Proceedings of an International Conference, Liverpool, 1990* (CRC Press, 1990)
- [7] N. Roussel, A thixotropy model for fresh fluid concretes: Theory, validation and applications. *Cement and concrete research* **36**(10), 1797–1806 (2006)
- [8] P. Coussot, Yield stress fluid flows: A review of experimental data. *Journal of Non-Newtonian Fluid Mechanics* **211**, 31–49 (2014)
- [9] D. Liu, Z. Zhang, X. Zhang, Z. Chen, 3d printing concrete structures: State of the art, challenges, and opportunities. *Construction and Building Materials* **405**, 133364 (2023)
- [10] S. El-Sayegh, L. Romdhane, S. Manjikian, A critical review of 3d printing in construction: Benefits, challenges, and risks. *Archives of Civil and Mechanical Engineering* **20**, 1–25 (2020)
- [11] H.A. Barnes, Thixotropy—a review. *Journal of Non-Newtonian fluid mechanics* **70**(1-2), 1–33 (1997)
- [12] S. Jarny, N. Roussel, R. Le Roy, P. Coussot, Modelling thixotropic behavior of fresh cement pastes from mri measurements. *Cement and Concrete Research* **38**(5), 616–623 (2008)
- [13] J. Tchamba, S. Amziane, G. Ovarlez, N. Roussel, Lateral stress exerted by fresh cement paste on formwork: laboratory experiments. *Cement and Concrete Research* **38**(4), 459–466 (2008)

- [14] CEN. Testing fresh concrete – part 8: Self-compacting concrete – slump-flow test. National adoption e.g., BS EN 12350-8:2019 (2019). URL <https://standards.iteh.ai/catalog/standards/sist/c868fc6c-71dc-466a-890a-f149d2f8f615/sist-en-12350-8-2019>
- [15] CEN/TC 104. Testing fresh concrete – part 9: Self-compacting concrete – v-funnel test (2010). URL <https://standards.iteh.ai/catalog/standards/cen/466570a0-196b-40b9-b3e0-fa0cb550100f/en-12350-9-2010>. Official versions in English, French, German
- [16] G.H. Tattersall, P.F. Banfill, *The rheology of fresh concrete*. Monograph (1983)
- [17] N. Roussel, *Understanding the rheology of concrete* (Elsevier, 2011)
- [18] A. Beris, J. Tsamopoulos, R. Armstrong, R. Brown, Creeping motion of a sphere through a bingham plastic. *Journal of Fluid Mechanics* **158**, 219–244 (1985)
- [19] B. Gueslin, L. Talini, B. Herzhaft, Y. Peysson, C. Allain, Flow induced by a sphere settling in an aging yield-stress fluid. *Physics of Fluids* **18**(10) (2006)
- [20] R. Biswas, D. Saha, R. Bandyopadhyay, Quantifying the destructure of a thixotropic colloidal suspension using falling ball viscometry. *Physics of Fluids* **33**(1) (2021)
- [21] T. Ferroir, H. Huynh, X. Chateau, P. Coussot, Motion of a solid object through a pasty (thixotropic) fluid. *Physics of Fluids* **16**(3), 594–601 (2004)
- [22] R.P. Chhabra, S.A. Patel, *Bubbles, drops, and particles in non-Newtonian fluids* (CRC press, 2023)
- [23] G.G. Stokes, et al., On the effect of the internal friction of fluids on the motion of pendulums (1851)
- [24] H. Tabuteau, P. Coussot, J.R. de Bruyn, Drag force on a sphere in steady motion through a yield-stress fluid. *Journal of rheology* **51**(1), 125–137 (2007)
- [25] S. van den Wildenberg, X. Jia, J. Léopoldès, A. Tourin, Ultrasonic tracking of a sinking ball in a vibrated dense granular suspension. *Scientific Reports* **9**(1), 5460 (2019)
- [26] H. Mohammad, B. Munshi, Experimental estimation of the settling velocity and drag coefficient of the hollow cylindrical particles settling in non-newtonian fluids in an annular channel. *The Canadian Journal of Chemical Engineering* **101**(11), 6632–6640 (2023)
- [27] M.M. Mroksa, A. Krztoń-Maziopa, Viscoelastic and shear-thinning effects of aqueous exopolymer solution on disk and sphere settling. *Scientific reports* **9**(1), 7897 (2019)

- [28] H. Koochi, J. Mac Intyre, M. Korhonen, A. Puisto, N. Maleki-Jirsaraei, M. Alava, Interaction between a free-falling sphere and structure dynamics in a heterogeneous thixotropic fluid. *Physics of Fluids* **35**(8) (2023)
- [29] A.A. Yazdi, G. D'Avino, Sedimentation and migration dynamics of a spherical particle in an elastoviscoplastic fluid near a wall. *Journal of Non-Newtonian Fluid Mechanics* **314**, 105004 (2023)
- [30] B. Gueslin, L. Talini, Y. Peysson, Sphere settling in an aging yield stress fluid: link between the induced flows and the rheological behavior. *Rheologica acta* **48**, 961–970 (2009)
- [31] B. Strybny, J. Link, M. Coenen, V. Vidal, M. Zuber, T. Schack, M. Haist, Mechanisms of air bubble rise in cement suspensions studied by x-ray analysis. *Construction and Building Materials* **457**, 139330 (2024)
- [32] G. Ovarlez, F. Bertrand, P. Coussot, X. Chateau, Shear-induced sedimentation in yield stress fluids. *Journal of Non-Newtonian Fluid Mechanics* **177**, 19–28 (2012)
- [33] M.G. Kleinhans, C.R. Jeukens, C.J. Bakker, R.M. Frings, Magnetic resonance imaging of coarse sediment. *Sedimentary Geology* **208**(3-4), 69–78 (2008)
- [34] M.A. Ferrari, A. Lugarini, A.T. Franco, Fully-resolved simulations of a sphere settling in an initially unstructured thixo-viscoplastic fluid. *Journal of Non-Newtonian Fluid Mechanics* **294**, 104574 (2021)
- [35] N. Roussel, G. Ovarlez, S. Garrault, C. Brumaud, The origins of thixotropy of fresh cement pastes. *Cement and concrete research* **42**(1), 148–157 (2012)
- [36] S. Dhar, T. Liberto, C. Barentin, T. Divoux, A. Robisson, Discrepancies in dynamic yield stress measurements of cement pastes. *Rheologica Acta* **63**(9), 657–672 (2024). <https://doi.org/10.1007/s00397-024-01465-9>
- [37] J.J. Thomas, H.M. Jennings, Materials of cement science primer: The science of concrete. Tech. rep. (2009). <https://doi.org/10.21985/N20N36>
- [38] R. Ladenburg, Über den einfluß von wänden auf die bewegung einer kugel in einer reibenden flüssigkeit. *Annalen der Physik* **328**(8), 447–458 (1907)
- [39] V. Fidleris, R. Whitmore, Experimental determination of the wall effect for spheres falling axially in cylindrical vessels. *British journal of applied physics* **12**(9), 490 (1961)
- [40] C.A. Schneider, W.S. Rasband, K.W. Eliceiri, Nih image to imagej: 25 years of image analysis. *Nature methods* **9**(7), 671–675 (2012)
- [41] V.A. Hackley, C.F. Ferraris, *Guide to rheological nomenclature: Measurements in ceramic particulate systems*, vol. 3 (Citeseer, 2001)

- [42] P.A. Durbin, G. Medic, *Creeping Flow* (Cambridge University Press, 2007), p. 108–131
- [43] P. Coussot, Q.D. Nguyen, H. Huynh, D. Bonn, Avalanche behavior in yield stress fluids. *Physical review letters* **88**(17), 175501 (2002)
- [44] M. Saadat, D. Mangal, S. Jamali, A rheologist's guideline to data-driven recovery of complex fluids' parameters from constitutive models. *Digital Discovery* **2**(4), 915–928 (2023)
- [45] A. Franck, Understanding rheology of structured fluids. Book of TA instruments pp. 1–17 (2004)
- [46] G. Kaya, F. Oytun, Rheological properties of injectable hyaluronic acid hydrogels for soft tissue engineering applications. *Biointerface Res. Appl. Chem* **11**, 8424–8430 (2020)
- [47] N. Roussel, A thixotropy model for fresh fluid concretes: Theory, validation and applications. *Cement and Concrete Research* **36**(10), 1797–1806 (2006). <https://doi.org/10.1016/j.cemconres.2006.05.025>
- [48] Y.M. Joshi, Perspective: Analysis of thixotropic timescalea. *Journal of Rheology* **68**(4), 641–653 (2024). <https://doi.org/10.1122/8.0000816>

# Supplementary Information

## S1: Schematic of experimental setup

Fig. S1 shows the schematic of the experimental setup used in this work. A vertical plastic tube, with a height of 550 mm and a diameter of 70 mm, is filled for each experiment with cement paste until 450 mm height. As measurements are done inside an isolated X-ray chamber, an electromagnetic setup is used to place and release the ball at the chosen time. A funnel is placed at the mouth of the cylindrical tube containing the cement paste, to ensure that the sphere falls in the middle of the cement paste. The observation region of the device has a height of only 300 mm, as shown in the figure.

## S2: Three dimensional fits of the steady state velocity of the falling balls

Fig. S2 shows the 3D fits of the ball velocity for the Cases I - IV (Eqns. 13, 15, 17 and 19 of main text). The three axes are the ball velocity, time (age of paste) and the ball radius. the input and output parameters are discussed in Section 6.1 of main text. The R-squared values in Case I to IV are 0.56, 0.70, 0.56 and 0.91 respectively. A value of R-squared closer to 1 represents a better fit.

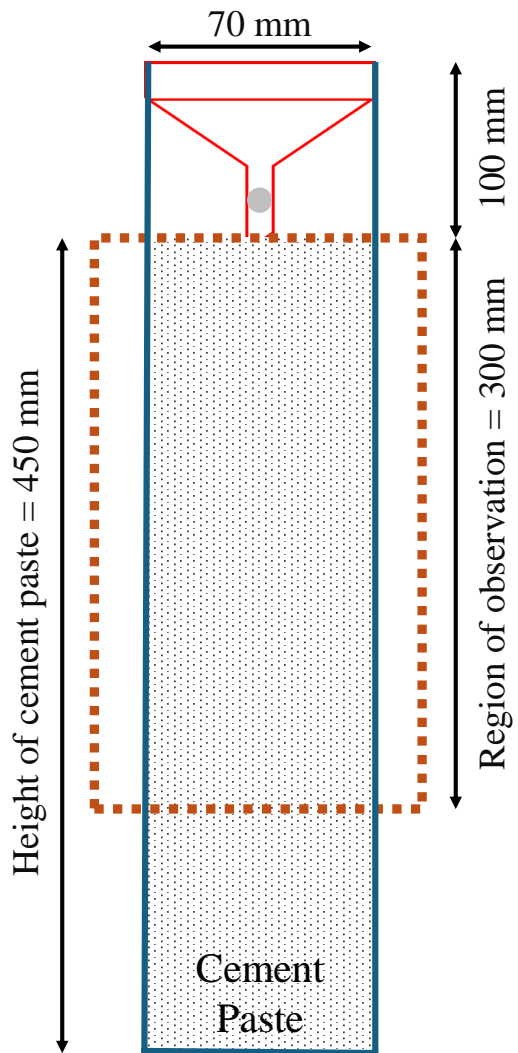


Fig. S1: Schematic of experimental setup inside an X-ray chamber. The tube has a height of 550 mm and a diameter of 70 mm, with a 100 mm funnel and a 300 mm observation region. The paste is filled up to a height of 450 mm.

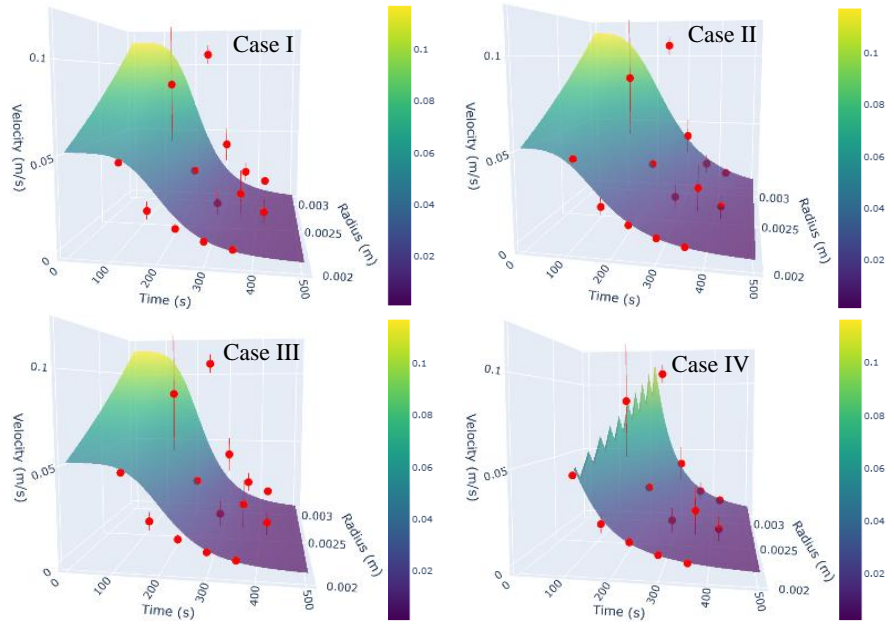


Fig S2: Three dimensional plots to fit Cases I to IV. The bars on the right represent the colour coding of the velocity. The three axes represent, the ball velocity, time (age of paste) at start of sphere falling, and ball radius.

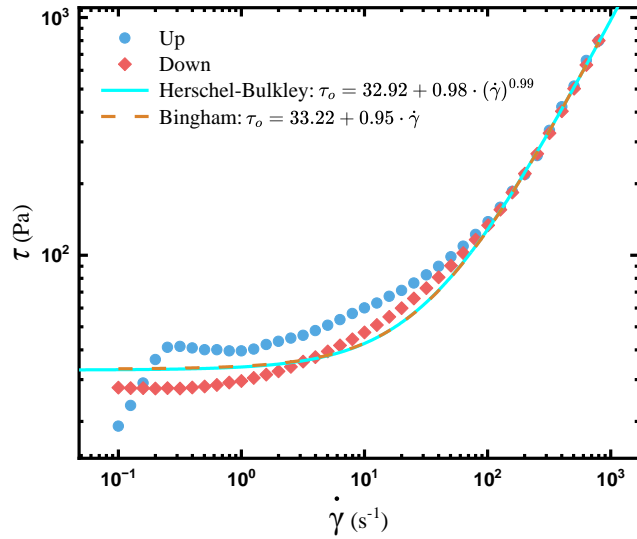


Fig S3: Cement paste shear stress  $\tau$  as a function of shear rate  $\dot{\gamma}$ , with Herschel Bulkley (cyan) and Bingham (orange) fits to identify dynamic shear stress  $\tau_o$ , from ramp down flow test.

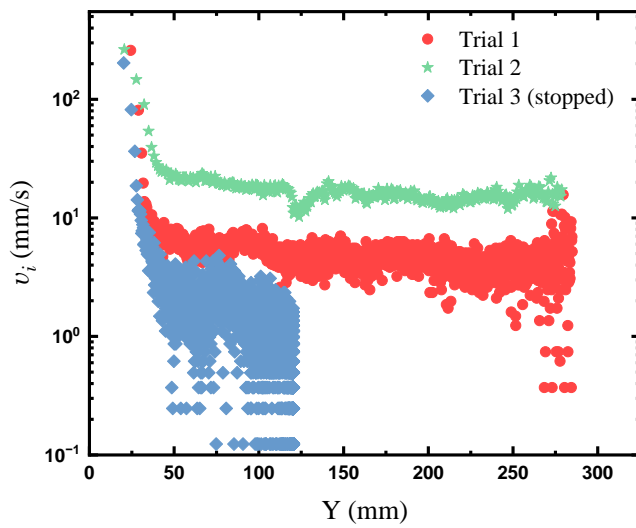


Fig S4: Instantaneous ball velocity  $v_i$  as a function of position for paste age of  $t = 420$  s, using a 2.5 mm ball. During trial 3 (blue diamonds), the ball stopped within the window of observation.